DOI: 10.1002/cphc.200900069

Physical–Chemical Properties and Transfection Activity of Cationic Lipid/DNA Complexes

Maria N. Antipina,*[a, c] Ingo Schulze,[b] Martin Heinze,[b] Bodo Dobner,[b] Andreas Langner,[b] and Gerald Brezesinski*[a]

Investigation of DNA interactions with cationic lipids is of particular importance for the fabrication of biosensors and nanodevices. Furthermore, lipid/DNA complexes can be applied for direct delivery of DNA-based biopharmaceuticals to damaged cells as non-viral vectors. To obtain more effective and safer DNA vectors, the new cationic lipids 2-tetradecylhexadecanoic acid-{2-[(2-aminoethyl)amino]ethyl}amide (C**I**) and 2-tetradecylhexadecanoic acid-2-[bis(2-aminoethyl)amino]ethylamide (C**II**) were synthesized and characterized. The synthesis, physical–chemical properties and first transfection and toxicity experiments are reported. Special attention was focused on the capability of C**I** and C**II** to complex DNA at low and high subphase pH values. Langmuir monolayers at the air/water interface represent a well-defined model system to study the lipid/DNA complexes. Interactions and ordering of DNA under Langmuir monolayers of the new cationic lipids were studied using film balance measurements, grazing incidence X-ray diffraction (GIXD) and X-ray reflectivity (XR). The results obtained demonstrate the ability of these cationic lipids to couple with DNA at low as well as at high pH value. Moreover, the observed DNA structuring seems not to depend on subphase pH conditions. An influence of the chemical structure of the lipid head group on the DNA binding ability was clearly observed. Both compounds show good transfection efficacy and low toxicity in the in vitro experiments indicating that lipids with such structures are promising candidates for successful gene delivery systems.

Introduction

A wide range of practical applications in life science is closely connected to supramolecular organization at the nanoscale. Self-assembling and ordering of DNA molecules at planar, oppositely charged surfaces is of particular interest for the preparation of biomaterials, functional nanostructures, DNA chips, biosensors and nanodevices.[1–5] Another important field requiring a deeper understanding of the mechanisms of DNA interactions with cationic lipids is medical gene therapy, which seems to be the most innovative method in the treatment of genetic and serious acquired diseases including cancer, AIDS, Parkinson's and Alzheimer's diseases and cardiovascular disorders.[6–8] Lipid/DNA complexes mimic the ability of natural viruses to transfect genetic material to the cell core. In contrast to the viral systems these complexes do not have immunogenic potential or restrictions with regard to the size of the delivered gene fragments.[9–11] However, cationic lipids and also other non-viral vectors such as polymers and peptides suffer from low transfection efficacy and pronounced toxicity. Further success will only be achieved by designing new compounds followed by in vitro tests of their transfection activity and cytotoxicity. Here we present new and cheap gene transfer vectors. The lipid part including the backbone is represented by long chain branched fatty acids which are essential for the stability of the complexes with DNA. The synthesis of two novel cationic lipids as well as the physical–chemical characterization of the new compounds organized as Langmuir monolayers at the air–water interface will be described. Special focus was put on the coupling of DNA with the monolayer resulting in a one-dimensional ordering of bio-macromolecules at the charged surface. Despite a large number of publications devoted to different aspects of DNA/cationic monolayer interaction,[12–21] the influence of the chemical structure of lipid molecules as well as of the monolayer phase state on the coupling behavior is not fully understood. Therefore, emphasis was placed on a detailed physical–chemical characterization of the novel amphiphilic compounds accompanied by biological testing. Successful delivery of DNA-based therapeutics requires a certain stability of the DNA/vector complex in the slightly acidic environment of the endosomes followed by in situ liberation of drugs in cytosole or nucleus, where the pH value is close to 7.[22] It has been already shown that the subphase pH value influences clearly the protonation state of the newly synthesized cationic lipids.[23] Thus, the other important question to be investigated is the perspective to use the novel compounds as pH-sensitive delivery vectors, that means to study in detail the effect of the subphase pH value on the physical–chemical properties of the

[a] *Dr. M. N. Antipina, Prof. Dr. G. Brezesinski*
Max Planck Institute of Colloids and Interfaces
Am Muehlenberg 1, 14476 Potsdam (Germany)
Fax: (+49) 331-567-9202
E-mail: brezesinski@mpikg.mpg.de

[b] *Dr. I. Schulze, M. Heinze, Prof. Dr. B. Dobner, Prof. Dr. A. Langner*
Institute of Pharmacy, Martin-Luther-University
Wolfgang-Langenbeck-Str. 4, 06120 Halle/S. (Germany)

[c] *Dr. M. N. Antipina*
Institute of Materials Research and Engineering
3 Research Link, 117602 (Singapore)
Fax: (+65) 687-275-28
E-mail: antipinam@imre.a-star.edu.sg

cationic lipid monolayers, on DNA adsorption and on the structure of the DNA/lipid complexes.

Results and Discussion

The cationic head groups of the newly synthesized lipids (Figure 1) are represented by oligoamines, which can be protonated and therefore positively charged or deprotonated/uncharged depending on the environmental pH value. To study the physical–chemical properties of these cationic lipids and their interactions with DNA, subphases with pH 4 and pH 8 were used to mimic closely the physiological conditions of lysosome and cytosol, respectively. The protonation properties of the novel compounds in dependence on the bulk pH value have been already studied.[23] According to the total reflection X-ray fluorescence (TRXF) experiments, 100% of the lipid molecules at the air–water interface are charged at pH 4 and ~40% of them have even two positive charges per head group. In contrast, pH 8 corresponds to the mostly deprotonated state of the monolayer, only 5% of the monolayer molecules have one positive charge in the head group. The titration curves are identical for both lipids studied independent of the head group structure.[23]

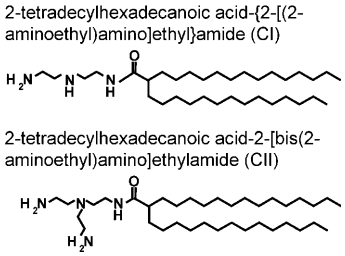

Figure 1. Chemical structures of the newly synthesized cationic lipids.

The pH-dependent protonation of the head group influences the pressure–area (π--A) isotherms of the pure monolayers (Figure 2). The large molecular areas, observed for the monolayers of C**I** and C**II,** indicate that they are in a fluid-expanded state at both investigated pH values. No evidence of lateral ordering was observed by grazing incidence X-ray diffraction (GIXD). Electrostatic repulsion between the protonated head groups leads to an expansion of the monolayer (shift to larger molecular areas) at pH 4 compared to the behavior at pH 8 which corresponds to a less charged state of the molecules at the interface. At low pH value, coupling of DNA to the C**I** or C**II** monolayers leads to a further expansion, especially at surface pressures below 20 mN m^{-1} giving evidence that DNA can penetrate into the monolayers. The location of the adsorbed DNA will be discussed later. On compression, a pronounced change of the slope of the isotherms indicates that the DNA is partly squeezed out of the lipid monolayer at higher surface pressures. In spite of a minor amount of protonated lipid head groups at pH 8, sufficient expansion of the monolayers in the presence of DNA shows that DNA interacts with the lipid monolayers of C**I** and C**II** under this condition. Thus, even the low surface charge density is sufficient for DNA coupling to these monolayers at the air–liquid interface.

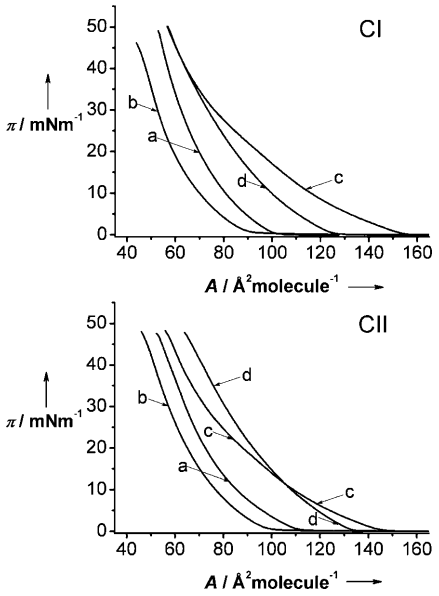

Figure 2. Pressure–area isotherms of the monolayers of C**I** (top), C**II** (bottom), on citric buffer, pH 4 (a), Tris buffer, pH 8 (b), citric buffer, pH 4, in presence of 0.1 mM DNA (c) and on Tris buffer, pH 8, in presence of 0.1 mM DNA (d).

It can be clearly seen (Figure 2, bottom) that in the presence of DNA above a pressure of 12 mN m^{-1} the monolayer of C**II** occupies more area at pH 8 than at pH 4. An explanation for this observation could be that the protonated, branched lipid head group interacts strongly with the DNA molecules so that upon squeezing-out of penetrated DNA a certain number of strongly interacting lipid molecules is lost into the subphase during compression of the film. This process is reversible.

As C**I** and C**II** form fluid monolayers, no ordered lipid structures were detected using GIXD. Nevertheless, GIXD was applied to study the one-dimensional periodicity in the adsorbed DNA layer. Schematic representation of DNA ordering under the monolayer surface together with a selected contour plot of the corrected X-ray intensities as a function of the in-plane and out-of plane scattering vector components Q_{xy} and Q_z of C**I** on a DNA containing subphase are shown in Figure 3. As it was already demonstrated elsewhere,[24] the lattice spacing of DNA depends on the pH value but is almost independent of the surface pressure if the lipid monolayer is in a condensed state. In contrast, the distance between the aligned DNA strands adsorbed to fluid lipid layers is clearly pressure-dependent, but not distinctly influenced by the pH value (Figure 4). The lateral ordering of DNA must be a result of two counteracting processes: 1) The electrostatic attraction of oppositely charged lipid head groups and DNA, and 2) the repulsion of like charged DNA molecules. Thus, in the case of condensed lipid layers the smaller amount of positively charged molecules in the monolayer on the supbhase at pH 8 does not allow DNA to pack so closely as on the pH 4 subphase due to a less effective charge compensation. In the case of fluid monolayers, the average surface charge density at any pH value is

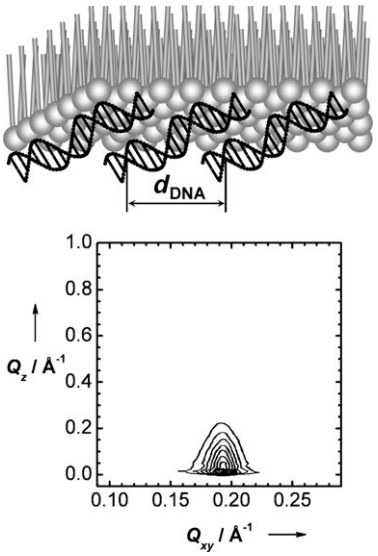

Figure 3. Molecular model of DNA ordering at the monolayer of the novel cationic lipids (top). Selected contour plot of corrected X-ray intensities as a function of the in-plane (Q_{xy}) and the out-of-plane (Q_z) scattering vector components of C**I** monolayer on 0.1 mM DNA solution in citric buffer, pH 4, at $\pi = 40$ mN m^{-1} (bottom).

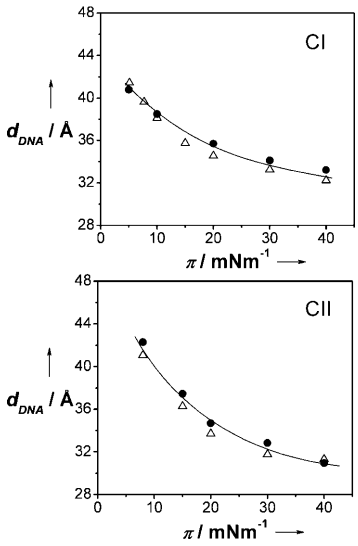

Figure 4. The lattice spacing between organized DNA strands (d_{DNA}) adsorbed at the monolayer of C**I** (top) or C**II** (bottom) as a function of the surface pressure π. The monolayer is formed on the subphase containing 0.1 mM DNA in citric buffer, pH 4 (-△-) or in Tris buffer, pH 8 (-●-).

smaller compared with condensed layers. Therefore, a tight packing of DNA molecules cannot be observed. The question arises: Why are the d-spacing values essentially the same at both pH values? In the case of pH 8 subphase, the initial approach of the biopolymer to the interface leads obviously to a further protonation of the lipid molecules which then in turn attract more DNA, so that at the end of the adsorption process similar charge densities can be expected in the monolayers at both pH values. The lattice spacing of DNA is also influenced by the structure of the lipid head group. According to our results, the branched polyamine head group in C**II** leads to larger d-spacing values at low pressure and smaller values at high pressure compared with the straight head group structure of C**I**.

Zwitterionic 1,2-dioleoylphosphatidylethanolamine (DOPE) as a helper lipid in cationic lipid/DNA formulations often promotes transfection efficacy.[25–26] Therefore, the interaction of DNA with Langmuir monolayers of binary mixtures of the new cationic lipids and DOPE was also studied (Figure 5). For both investigated compounds, the DNA lattice spacing is found to

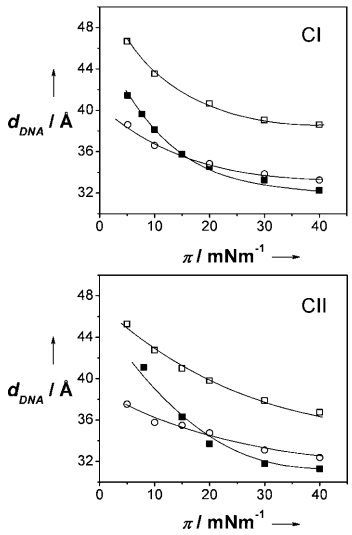

Figure 5. The lattice spacing between organized DNA strands (d_{DNA}) adsorbed at mixed monolayers composed of DOPE and C**I** (top) or C**II** (bottom) as a function of the surface pressure π. Monolayer compositions: cationic lipid: DOPE = 1:1 (-○-), cationic lipid : DOPE = 1:3 (-□-). Control data for monolayers of the pure cationic lipids (-■-). The monolayers are formed on the 0.1 mM DNA solution in citric buffer, pH 4.

be slightly less pressure-dependent using mixed monolayers than pure cationic layers. If three quarters of the monolayer area are occupied by DOPE, the distance between ordered DNA molecules is on average 7 Å larger compared with the 1:1 binary mixture. At low surface pressure values (below 20 mN m^{-1}), the DNA strands are slightly denser packed at the 1:1 cationic lipid/DOPE mixed monolayer than at the pure cationic layers. This result cannot be explained in terms of charge compensation as the π–A isotherms of the binary mixtures on the DNA containing subphase (data not shown) and the X-ray reflectivity studies give evidence for a penetration of DNA molecules into the film. On the other hand, we have no clear information about the miscibility behavior in the mixed films. Since both compounds form liquid-expanded monolayers, full miscibility can be expected on the pure subphase. Interaction of DNA with the charged species could lead to a partial phase separation in the mixed layer. Such an assumed phase separation could be pressure-dependent. An assumed liquid–liquid phase separation results in a higher surface charge density in the regions formed by the cationic lipid molecules, however the charge density cannot be higher compared with that of the pure cationic lipid layer. The only reasonable explanation seems to be an enhanced interaction owing to sterical reasons

because the presence of a certain number of DOPE molecules allows the denser packing of DNA.[27–29]

Time-dependent experiments give evidence that the coupling of DNA to the mixed monolayers is a dynamic process, thus d_{DNA} depends both on surface pressure and time. The results shown in Figure 6 were obtained using the following protocol: the C**II** monolayer was first compressed until the desired surface pressure and X-ray diffraction data were measured.

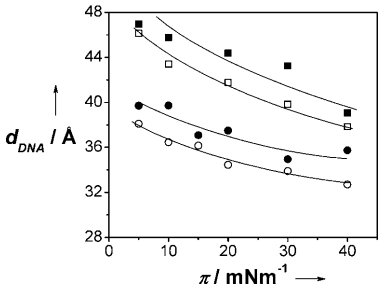

Figure 6. Dynamics in coupling of DNA to the mixed monolayers. Interaxial repeat distance d_{DNA} between ordered DNA strands versus monolayer surface pressure π. Monolayer compositions: C**II** : DOPE = 1:1 (-○-), data recorded after 1 hour (-●-); C**II** : DOPE = 1:3 (-□-), data recorded after 1 hour (-■-). Subphase conditions: 0.1 mM DNA solution in citric buffer, pH 4.

After one hour of incubation of the monolayer at fixed surface pressure, the X-ray experiment was repeated. Figure 6 shows that the interaxial repeat distance of DNA sublattices is on average 2 Å larger after one hour of incubation indicating that the reorganization of adsorbed DNA is a quite slow process, showing that even slow compression of the mixed monolayer leads to a non-equilibrium state. The adsorbed DNA strands, which are compressed together with the lipid layer, are obviously too tightly packed. The balancing of the forces leads to the reorganization in the adsorption layer. This reorganization might be connected with a partial desorption followed by a new adsorption process.

All GIXD studies of DNA organization at the surfaces of C**I** and C**II** monolayers demonstrate clearly the pressure dependence of d_{DNA}. The possible reasons of this phenomenon could be either changes in the monolayer surface charge density leading to further adsorption and reorganization of DNA, or a simple rapprochement of coupled DNA strands together with the lipid molecules by compression of the layer. To clarify this question, GIXD investigations of DNA ordering were performed for the C**II** monolayer in the following way: the surface pressure was adjusted not via compression of the film but by adding of an appropriate amount of the lipid on the DNA containing subphase. The results are shown in Figure 7. Good agreement of the data obtained in both experiments supports the first assumption, thus the driving force of DNA organization and alignment under the monolayers of the novel cationic lipids is the surface charge density.

Figure 8 displays X-ray reflectivity data of C**I** and C**II** monolayers on various subphases at 30 mN m^{-1} together with the corresponding free-form fits (solid line). Reflectivity from the monolayer on the pure buffer interface is clearly different from

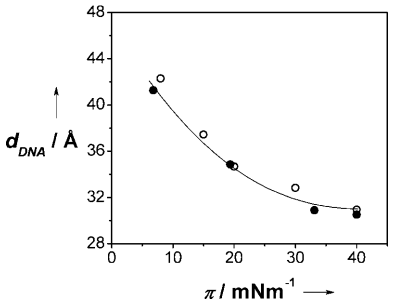

Figure 7. The lattice spacing between organized DNA strands (d_{DNA}) under the C**II** monolayer as a function of the surface pressure π. Surface pressure π is adjusted via compression of the monolayer (-○-), via adding of an appropriate lipid amount on the DNA containing subphase (-●-).

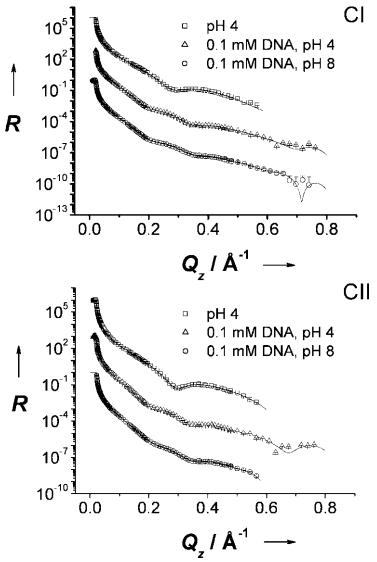

Figure 8. X-ray reflectivity data (-□-) and fit (—) obtained using 23 spline functions for the C**I** and C**II** Langmuir monolayers on various subphases (indicated).

that on the DNA containing solutions. The obtained electron density profiles (Figure 9) show the contribution of adsorbed/penetrated DNA. Subsequently, the electron density profiles were chemically interpreted by applying prior information such as the surface area of the molecule. A defined "box model" could only be used for the lipid monolayers on the pure buffer subphase with sufficient accuracy. The main reason for this problem seems to be that the DNA adsorption layer is not homogeneous. We describe therefore the electron density profiles by assuming a symmetrical electron density distribution in the hydrophobic chain region and a defined roughness between the hydrophilic region, containing the lipid head groups and adsorbed/penetrated DNA molecules, and the subphase. Assuming the tail group to be symmetric and constraining the number of electrons in tails (233 electrons) results in a unique electron density distribution for the tails. The value for the full width at half maximum (fwhm) of the chain electron density distribution translates directly to the thickness of the hydrophobic region. Figure 10 shows the chemical structure of

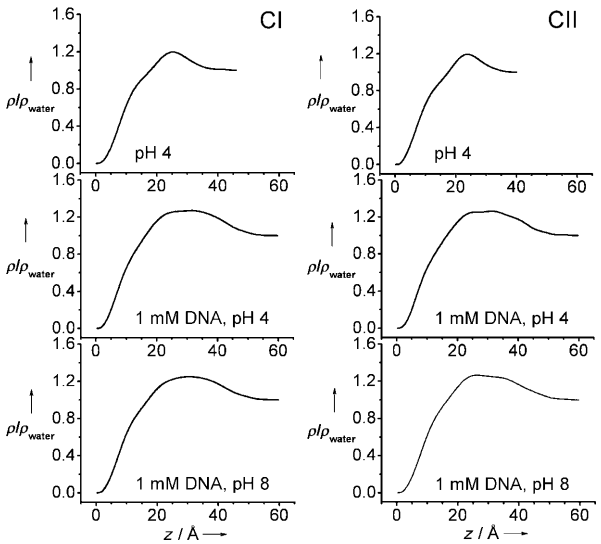

Figure 9. Electron density ρ profiles obtained from the reflectivity data of C**I** and C**II** on the different subphases (indicated).

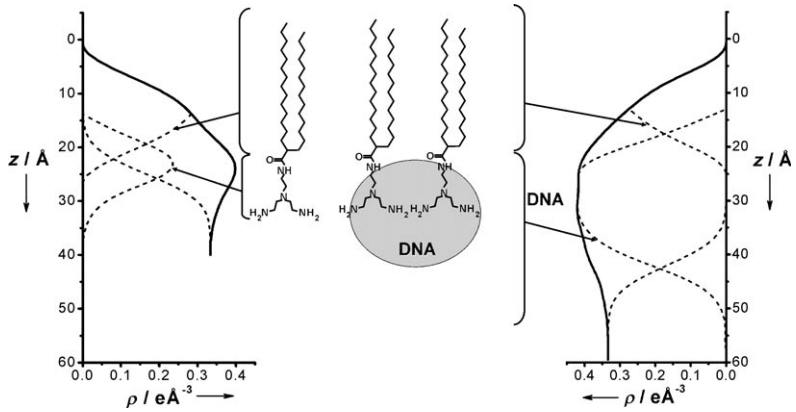

Figure 10. Electron density profiles of C**II** on the pure buffer (left) and on the DNA containing subphase (right). The dashed lines represent the contributions of the hydrophobic and hydrophilic parts and the roughness of the interface between the coupled system and the subphase.

the C**II** molecules together with a schematic representation of a DNA strand adsorbed to and partly penetrated into the head group region. The electron density profiles (solid lines) obtained for the C**II** monolayer on the pure subphase (left) and the subphase containing DNA (right) are shown with the corresponding contributions of the substructures (dashed lines). Parameters (area per molecule and number of electrons in the hydrophobic part) used for the fits and thicknesses of the two parts obtained from the observed electron density profiles are presented in Table 1. The results show that the thicknesses of the hydrophobic region for C**I** and C**II** on the pH 4 buffer subphase are very similar and typical for liquid chains. The head group region of C**I** is about 1 Å thicker than that of C**II** showing that the orientation of the head groups is slightly different. On the other hand, a comparison of the number of electrons in the head group region with the number of electrons obtained from the fit shows that the C**I** head group is by far more hydrated than the C**II** head group. The hydrophilic part of the film is sufficiently thicker if DNA is present in the aqueous solution (Figures 9 and 10, and Table 1). The thicknesses of the liquid alkyl chain layer on the DNA-containing subphases is for both pH values smaller compared with a system of pure buffer subphases. This is reasonable taking into account that the molecular areas on the DNA solutions are larger. The observed trend is in good agreement with the estimated thickness using $z = MW/(N_A \cdot A \cdot \rho)$ with MW as the molecular weight of the hydrophobic chains, N_A the Avogadro number, A the area per molecule and ρ the density of polyethylene (0.9 g cm^{-3}).[23] The thickness of the hydrophilic part of the coupled layers (approximately 24 Å) has been also determined from the fwhm of the corresponding electron density profiles. The comparison with the diameter of the B-form double-stranded DNA, which is proved to be 20 Å under physiological conditions,[30–31] shows that essentially one DNA layer is coupled to the head group region. Since the DNA layer is not densely packed (see GIXD results), the effective thickness of the hydrophilic part of the coupled lipid/DNA layer, determined by the reflectivity experiments, is a little smaller than the total thickness of the lipid head groups and the DNA. Additionally, partial penetration of DNA into the lipid head group region has also to be taken into account. Thus, DNA interactions with the monolayers of the novel cationic lipids result in the formation of a biopolymer layer with a one-dimensional periodicity underneath the lipid head groups. Assuming that the hydration state of the lipid head groups is the same at both pH

Table 1. Constrains and results of fitting electron density profiles to the reflectivity data of C**I** and C**II** Langmuir monolayers at $\pi = 30$ mN m^{-1}, using a free-form model. N_e is the number of electrons in the hydrophobic and hydrophilic parts, respectively. The number of electrons in the hydrophobic part and the molecular areas taken from the isotherms have been fixed to constrain the fit.

Lipid	CI			CII		
Subphase	pH 4	DNA, pH 4	DNA, pH 8	pH 4	DNA, pH 4	DNA, pH 8
Molecular area [Å^2·molecule^{-1}]	63	77	74	65	74	81
N_e (hydrophobic/hydrophilic)	233/206	233/792	233/727	232/162	232/729	233/811
Thickness hydrophobic [Å]	12.9	11.5	11.5	12.7	12.1	10.5
Thickness hydrophilic [Å]	10.6	24.7	24.0	9.3	23.8	24.3
Roughness [Å]	4	4	4	4	4	4

values, the estimated number of electrons in the hydrophilic region of the coupled layers shows that the amount of DNA adsorbed to C**I** is on the pH 4 subphase slightly larger than on the pH 8 subphase. However, the difference in the number of electrons is much smaller than expected from the difference in the experimentally determined protonation state.[23] This demonstrates again that the approaching DNA increases the protonation state of the C**I** molecules at pH 8. Surprisingly, for C**II** an even larger number of electrons in the hydrophilic part was observed for pH 8 compared with pH 4.

Figure 11 shows the difference between the electron density profiles observed on the pure buffer and on the DNA-containing buffer. The electron density of the fluid chain region is practically not influenced by DNA adsorption. The observed small difference in the lipid head group region indicated a partial penetration of DNA. For C**I**, a clear difference in the electron density profile difference on the pH 4 and pH 8 subphases can be seen, whereas the same profile has been observed for C**II** on both subphases. This shows that the lipid with the branched head group structure is able to attract the same amount of DNA at both pH values indicating that the branched head group is efficiently protonated on the pH 8 subphase by the coupled DNA. In the case of the C**I** monolayer, the straight structure of the lipid head groups seems to hamper this protonation process, and a smaller amount of DNA is adsorbed at pH 8 compared to pH 4.

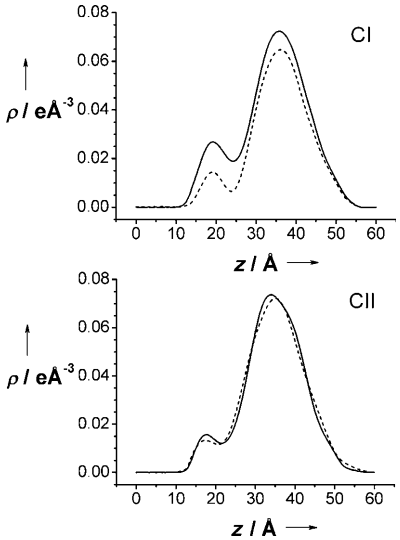

Figure 11. Differences in the electron density profiles on DNA containing subphase and on the pure buffer solution versus film thickness. Subphase pH conditions: pH 4 (—), pH 8 (--). The corresponding electron density profile of C**I** or C**II** on the pure buffer has been subtracted.

The sizes of liposomes and lipoplexes used for the biological experiments were measured by dynamic laser light scattering using different liposome/DNA charge ratios (from 0.5:1 to 2:1). The *z*-average values of lipoplexes vary within the range 160–400 nm. For both samples, lipoplexes with the highest *z*-average value exhibit high transfection efficiencies. Interestingly, the lipoplexes with the smallest size are less effective in terms of transfection. The calculated polydispersity index (PDI) values suggest a polydisperse distribution. The data are listed in Table 2.

Figure 12 summarizes the in vitro gene delivery efficacies of the lipids C**I** and C**II** in LLC PK1 cells. In these experiments, the cationic liposomes were prepared in combination with an equimolar amount of DOPE as the co-lipid. pCMV Sport β-Gal plasmid DNA was used as the reporter gene. The liposome/DNA charge ratios (±) were varied from 0.5:1 to 2:1 and the transfection efficiencies were detected with the *o*-nitrophenyl-β-*d*-galactopyranoside (ONPG) assay. Both liposome preparations were able to transfect the LLC PK1 cells. The results show that charge ratios near 1:1 (±) are the best for high transfection of plasmid DNA whereas more positive or negative charge in the lipoplexes leads to less transfection. These experiments show also that the head group structure of the lipids has no influence on the activity maximum. Only the optimal charge ratios are slightly different.

Figure 13 summarizes the in vitro viability of the LLC PK1 cells. 3-(4,5-Dimethylthiazol-2-yl)-2,5-diphenyltetrazolium bromide (MTT) based assays were performed using lipoplexes with different liposome/DNA charge ratios. In both cases, percent cell viabilities of the samples were found to be remarkably high. Surprisingly, enzyme activity using charge ratios of 0.5:1 and 1:1 (±) were observed although the cell viability was not statistically significantly influenced. Only the samples with charge ratios of 1.5:1 and 2:1 (±) decreased the cell viability. These results demonstrate that successful transfection is not coercible connected with increased toxicity.

Conclusions

The cationic lipids 2-tetradecyl-hexadecanoic acid-{2-[(2-aminoethyl)amino]ethyl}amide (C**I**) and 2-tetradecyl-palmitic acid-2-[bis(2-aminoethyl)amino]ethylamide (C**II**) were synthesized for further application as DNA delivery vectors. The capability of the new compounds to bind DNA was investigated at acidic and alkaline pH values to model physiological conditions of the transfection process. Coupling of DNA with the novel lipids was studied using Langmuir monolayers as a model system. It was shown that the subphase pH value influences the physical–chemical properties of the monolayers of the investigated

Table 2. Size measurements of liposomes and lipoplexes.

Sample		C**I**/DOPE 1:1 (n/n)		C**II**/DOPE 1:1 (n/n)	
		z average [nm]	PDI	*z* average [nm]	PDI
Liposomes		107 ± 2	0.252 ± 0.012	95 ± 2	0.313 ± 0.015
Liposome/DNA–charge ratio (+/)	0.5:1	258 ± 7	0.408 ± 0.013	211 ± 4	0.367 ± 0.032
	1:1	262 ± 4	0.424 ± 0.014	205 ± 4	0.387 ± 0.007
	1.5:1	215 ± 2	0.413 ± 0.017	375 ± 3	0.475 ± 0.021
	2:1	166 ± 2	0.330 ± 0.021	217 ± 3	0.405 ± 0.002

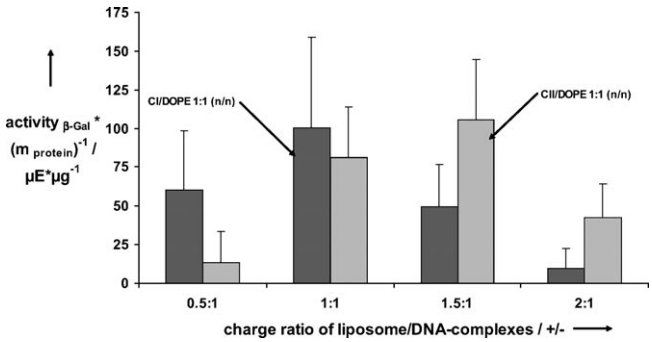

Figure 12. In vitro transfection efficiencies of lipids **CI** and **CII** in LLC PK1 cells using DOPE as co-lipid (at a lipid/DOPE molar ratio of 1:1) Microunits of β-Galactosidase related to the cell protein concentration were plotted versus the liposome to DNA (±) charge ratios. The transfection values shown are the average of five experiments carried out on three different days.

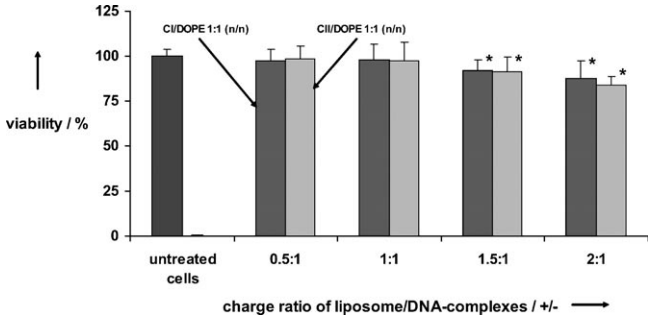

Figure 13. MTT-based cellular cytotoxicities of lipids **CI** and **CII** in LLC PK1 cells using DOPE as co-lipid (at a lipid/DOPE molar ratio of 1:1). The percent cell viability is plotted versus the liposome/DNA (±) charge ratio. The cell viability values shown are the average of five experiments carried out on three different days. Statistical analyses were carried out with $p < 0.05$, one way ANOVA and Bonferoni's multiple comparison tests.

lipids in absence and in presence of DNA. DNA coupling to the monolayers of the novel compounds was detected using film balance measurements, GIXD and X-ray reflectivity studies. All applied techniques give evidence for lipid complexation with DNA at pH 4 and pH 8. Moreover, no differences in the one-dimensional periodicity of ordered DNA strands were observed in dependence of the bulk phase pH conditions. In addition, very similar contribution of adsorbed DNA to the electron density profile of the lipid films was found at both investigated pH values. The results obtained let to suppose that further protonation of the amines in the lipid head groups occurs due to the approach of DNA to the air/water interface at pH 8, that in turn favors binding of DNA. The influence of the lipid head group structure on the coupling ability was also shown. Indeed, interactions of DNA with lipids having a branched head group structure (**CII**) seem to be stronger. Furthermore, at alkaline pH the branched polyamine chains were found to promote DNA adsorption more sufficient than the straight ones.

Both compounds show in combination with the helper lipid DOPE good transfection efficacy and low toxicity in the in vitro experiments indicating that lipids with such structures are promising candidates for successful gene delivery systems.

Experimental Section

Materials: For monolayer experiments, Milli-Q Millipore water with a specific resistance of 18.2 MΩ cm was used. 1,2-Dioleoylphosphatidylethanolamine (DOPE) and all chemicals for the preparation of buffers were obtained from Sigma–Aldrich (Germany). Deoxyribonucleic acid (DNA) used in the monolayer experiments was purchased from Sigma (Taufkirchen, Germany) and is a highly polymerized natural product originating from calf thymus. The sample was used without further purification. To minimize the danger of DNA denaturation, all experiments have been performed at 20 °C and only fresh solutions of 0.1 mM DNA containing 1 mM NaCl were used. Sodium chloride (obtained from Fluka) for the DNA solution was heated up to 600 °C to reduce the content of potential organic impurities. The monolayer experiments were performed either on citric buffer containing 50 mM $C_6H_8O_7$ and adjusted to pH 4 with NaOH, or on 10 mM Tris buffer, pH 8, containing 50 mM NaCl.

Synthesis of Compounds **CI** and **CII**: A keystep in the synthesis of the new cationic lipids was the preparation of 2-tetradecylhexadecanoic acid. This compound was synthesised by a double alkylation reaction of malonic acid ester with tetradecyl bromide followed by saponification and decarboxylation. The preparation of the monotetradecyl malonic acid ester was realized according to a published method.[32] The crude tetradecyl malonic acid ester was purified by column chromatography using silica gel 60 and heptane/ether as eluent. In a second step the purified ester, after deprotonation with sodium hydride, was alkylated again with tetradecyl bromide using xylene as solvent in a modified procedure of Breusch et al.[33] Saponification of the ester with potassium hydroxide in 95% ethanol leads to the corresponding ditetradecyl malonic acid which was afterwards heated up to 150 °C yielding the crude 2-tetradecylhexadecanoic acid. The purification of the branched fatty acid was performed by column chromatography using silicagel 60 and heptane/chloroform as eluent. The structure and purity of the acid was checked by mass spectrometry and ^{1}H NMR spectroscopy: M-($C_{30}H_{60}O_2$) = 452.8 g mol^{-1}; m.p. 63–64 °C; ^{1}H NMR ($CDCl_3$, 400 MHz): $\delta = 0.88$ (2t, 6H, $-CH_3$), 1.2–1.36 (m, 44H, chain), 1.48 and 1.66 (2 m, 4H, [$-CH_2-$CH$-CH_2-$]), 2.25 (m, 1H, [$-$CO$-CH=$]), 10.9 (m, 1H, $-OH$); MS (70 eV): *m/z* (%): 452 (30) [M^+], 484 (56) ($M^+-C_2H_4$, $-C_{12}H_{24}$). The carboxylic group of the branched fatty acid was then transformed into **CI** and **CII** via acid chloride by reaction with the corresponding amines: 2.5 mmol (1.0 g) of 2-tetradecylhexadecanoic acid were poured into 5 mL thionylchloride. The mixture was allowed to stand overnight at room temperature resulting in a clear solution which was then evaporated to remove the remaining thionyl chloride. For further purification the crude acid chloride was dried in vacuum over potassium hydroxide. The acid chloride was then dissolved in 10 mL dry chloroform. Mixtures of 25 mmol (2.58 g) bis(2-aminoethyl)amine and 2.5 mmol (0.25 g) triethylamine (for compound **CI**), respectively, 25 mmol (3.6 g) tris(2-aminoethyl)amine and 2.5 mmol (0.25 g) triethylamine (for compound **CII**) in 10 mL dry chloroform were dropped into the acid chloride solution with stirring and cooling in an ice bath. The mixture was stirred 2 h at room temperature and poured into crushed ice. The organic layer was separated, washed with water and dried over sodium sulphate. The solvent was evaporated and the crude product crystallized from heptane. The compounds were characterized by electrospray mass spectrometry (ESI-MS), elemental analysis and ^{1}H NMR spectroscopy.

CI: $C_{34}H_{71}N_3O$, 537.93 g mol^{-1}; m.p. 96–99 °C; ESI-MS *m/z*: 539 [$M^+ + H$], calcd.: C 75.91, H 13.30, N 7.81; found: C 76.35, H 13.20, N 7.11; ^{1}H NMR (400 MHz, $CDCl_3$): $\delta = 0.84$ (m, 6H, 2[$CH_3(CH_2)_{13}-$]), 1.2–1.5 (m, 54H, 2[$CH_3(CH_2)_{13}$, [H_2N-]), 2.62–2.67 (m, 4H,

[$H_2NCH_2CH_2NH$–],[-$HNCH_2CH_2NH$–]), 2.78–2.88 (m, 2H, [$H_2NCH_2CH_2NH$–]), 3.0–3.08 (m,1H, [–CH–]), 3.38–3.40 (m, 2H, [–$NHCH_2CH_2NHCO$–]), 4.1–4.2 (m, 2H, 2[–NH–]), 6.50–6.55 (m, 1H, [–NHCO–]).

CII: $C_{36}H_{76}N_4O$, 581.02 g mol^{-1}; m.p. 73–75 °C; ESI-MS *m/z*: 582 [M^+ + H], calcd.: C 74.42, H 13.18, N 9.64; found: C 74.32, H 13.11, N 9.70; ^{1}H NMR (400 MHz, $CDCl_3$): $\delta = 0.85$ (t, 6H, 2[$CH_3(CH_2)_{15}$–]), 1.21–1.57 (m, 64H, 2[$CH_3(CH_2)_{15}$–], 2[H_2N–]), 2.00–2.14 (m, 4H, 2[$H_2NCH_2CH_2$–]), 2.53–2.58 (m, 4H, 2[$H_2NCH_2CH_2$–]), 2.78 (t, 2H, [–NCH_2CH_2NH–]), 3.13–3.20 (m, 1H, [–CH–], 3.29–3.34 (m, 2H, [–NCH_2CH_2NH–]), 7.06 (s, 1H, [–CONH–]).

Monolayer Experiments: For monolayer experiments, 1 mM stock solutions of each cationic lipid were prepared in chloroform (Merck, Germany; purity > 99.8%). The necessary amount of the corresponding solution was placed onto the air/water interface by a microsyringe and allowed to relax for 10 min before compression for complete evaporation of the solvent. If DNA was present in the aqueous solution, the monolayer on the interface was incubated for one hour before experimental data were collected. The pressure/area (π–*A*) isotherms were recorded during compression of the monolayer on the computer-interfaced Langmuir trough (R&K, Potsdam, Germany). The compression rate of the films was approximately 2 Å^2 molecule^{-1} min^{-1}. The setup is equipped with a Wilhelmy balance to measure the monolayer surface pressure π and has a temperature control system. The subphase temperature was maintained at 20 °C with an accuracy of ±0.1 °C. Each film balance measurement was repeated at least five times and all recorded isotherms showed a good reproducibility.

X-ray Experiments: Grazing incidence X-ray diffraction (GIXD) and specular X-ray reflectivity (XR) measurements were performed using the liquid surface diffractometer (undulator beamline BW1) at HASYLAB, DESY, Hamburg, Germany.[34–38] The Langmuir trough is located in a thermostated, tightly closed and He-flashed container. A monochromatic beam ($\lambda = 1.304$ Å) from a beryllium (002) crystal strikes the water surface at an angle of 0.11° equal to 85% of the critical angle of total external reflection of water for this X-ray wavelength. A linear position sensitive detector (PSD) (OED-100 M, Braun, Garching, Germany) with a vertical acceptance $0 < Q_z < 1.27$ Å^{-1} was used for recording the diffracted intensity as a function of both the vertical [$Q_z \approx (2\pi/\lambda)\sin(\alpha_f)$] and the horizontal [$Q_{xy} \approx (4\pi/\lambda)\sin(\Theta)$] scattering vector components. α_f is the vertical and 2Θ is the horizontal scattering angle. The horizontal resolution of 0.008 Å^{-1} was determined by a Soller collimator mounted in front of the PSD. The accumulated position-resolved counts were corrected for polarization, effective area and Lorentz factor. Model peaks taken as a Lorentzian in the in-plane direction and a Gaussian in the out-of-plane direction, respectively, were least-square fitted to the measured intensities. If DNA adsorbs to a Langmuir monolayer and forms a one-dimensional periodicity, a diffraction peak ascribable to DNA lateral ordering appears at low Q_{xy} values.[39] Assuming that DNA adsorbs to the lipid monolayer as aligned cylinders, it is possible to calculate the lattice spacing (d_{DNA}) as a distance between neighboring DNA helixes by $d = 2\pi/Q_{xy}$, where Q_{xy} is the maximum of the Lorentz curve.

Using a NaI scintillation detector, the X-ray reflectivity was measured as a function of the vertical incidence angle, α_i, with the geometry, $\alpha_i = \alpha_f = \alpha$, where α_f is the vertical exit angle of the reflected X-rays. The incidence angle, α_i, was varied in the range 0.05°–5°, corresponding to a range of 0.01–0.85 Å^{-1} of the vertical scattering vector component $Q_z = (4\pi/\lambda)\sin(\alpha)$. The background scattering from, for example, the subphase was measured at $2\theta_{hor} = 0.7°$ and subtracted from the signal measured at $2\theta_{hor} = 0°$. The X-ray footprint area on the sample is inversely proportional to the incident angle of the X-rays.[40–41] Irrespective the usual phase problem of X-ray crystallography, the normalized reflectivity, $R(Q_z)/R_F(Q_z)$, where $R_F(Q_z)$ is the Fresnel reflectivity from an ideal smooth surface, can usually be inverted to yield the laterally averaged electron density, $\rho(z)$, as a function of the vertical *z* coordinate. The inversion of $R(Q_z)/R_F(Q_z)$ to yield $\rho(z)$ can be performed either by a model-independent method or by using a box model based on the molecular structure.[42–47] The model-free method is based on writing $\rho(z)$ in terms of cubic-spline functions $\rho(z) = \Sigma\alpha_i B_i(z)$, where *i* changes from 1 to *N* and *N* is determined by the accessible Q_z range via the sampling theorem, and least-squares fitting a profile for agreement between the corresponding model reflectivity and the measured reflectivity. Subsequently, the obtained electron density profile has to be chemically interpreted by applying prior information such as the surface area of the molecule and constraining the number of electrons in the different parts of the monolayer molecules.

Especially for heterogeneous monolayers, one has to keep in mind that the reflectivity is an average over the footprint area. XR provides information about an average structure projected onto the vertical *z* axis and contains also contributions from the subphase. In contrast, GIXD experiments probe only the parts of a monolayer with crystalline order.

Preparation of Liposomes: A chloroform solution of the pure cationic lipid (**CI** or **CII**) was combined with a chloroform solution of DOPE (BioChemica®). The mixtures were dried under reduced pressure to remove the chloroform, and the dried film was vacuum desiccated for 3 h. The lipid film was dissolved in distilled water at room temperature to a final concentration of 2 mg lipid per milliliter sample. The film was allowed to swell in a water bath at 45 °C for at least 15 min. Subsequently, the lipid formulations were vortexed and sonicated to clarity in a bath sonicator.[48–50] The samples were stored in the refrigerator at 4 °C before use.

Cells and Plasmid: LLC PK1 cells (ATCC® CL-101) were cultured in 75 cm^2 tissue culture flasks in Medium 199 (Gibco®BRL) adjusted to contain 2.2 g L^{-1} sodium bicarbonate, 10% fetal bovine serum (FBS) and 0.05 mg mL^{-1} gentamycine at 37 °C and 5% CO_2.[51] The cells were grown confluent and were regularly split twice a week. Only cells that had undergone fewer than 30 passages were used for transfection and MTT experiments. pCMV Sport β-Gal (Gibco®BRL) was isolated from Escherichia coli DH5α (Invitrogene life technologies) using a Quiagen plasmid mega kit (Quiagen™) following the manufacturer's instructions.[52] DNA with an $OD_{260}/OD_{280} = 1.94$ was used for the experiments.

Transfection Biology and Toxicity Assay: 24 h before transfection, cells were seeded into a 96 well plate at $1{\cdot}10^4$ cells/well. Lipoplex mixtures were prepared by combining plasmid DNA (0.1 μg per well) with varying amounts of cationic liposome suspension in plain Medium 199 (Gibco®BRL). The samples were incubated for 15 min at room temperature (total volume up to 40 μL/well). The charge ratios (±) were varied from 0.5:1 to 2:1. During this time, cells were washed once with phosphate-buffered saline (PBS). The complexes were then added to the cells. After 4 h of incubation, 60 μL of Medium 199 was added to the cells in a way that the final concentration of FBS reached 10%. The medium was refreshed after 24 h and the reporter gene activity was estimated after 48 h. For that, the cells were washed with phosphate buffered saline (PBS), lysed for 15 min in lysis buffer (5 mM Chaps in 50 mM Hepes buffer). The solution was taken out of the wells, reunited in safe-lock tubes (Eppendorf®), centrifuged and stored on ice. It was pipetted again in a 96 well plate and substrate solution

[1.33 mg mL^{-1} of *o*-nitrophenyl-β-galactopyranoside (ONPG), 2 mM $MgCl_2$, 100 mM β-mercaptoethanol in 0.2 M sodium phosphate, pH 7.3] was added and incubated for 30 min at 37 °C. The reaction was stopped with 1 M sodium carbonate. Absorption at 405 nm was converted to β-galactosidase units using a calibration curve obtained with pure commercial β-galactosidase enzyme.[53] Protein concentration was detected with bichinonic acid reaction.[54] Absorption at 570 nm was converted by using a calibration curve from bovine serum albumin.

Cytotoxicities of the liposomes were assessed by the 3-(4,5-dimethylthiazol-2-yl)2,5-diphenyltetrazolium bromide (MTT) reduction assay.[55] The cytotoxicity assay was performed as the transfection described above. MTT was added after refreshing the medium (24 h after addition of the samples). The results were expressed as percent viability $=([A_{540}(\text{treated cells})-\text{background}]/[A_{540}(\text{untreated cells})-\text{background}])\cdot 100$. All experiments were carried out six times. Every experiment was repeated three to five times on different days.

Size Measurements: The sizes of liposomes and lipoplexes were measured in distilled water by photon correlation spectroscopy on a HPPS-ET (Malvern, U.K.) with sample refractive index of 1.25 and a viscosity of 0.8872 N·s m^{-2} at 25 °C. Lipoplexes were measured with 2.5 μg DNA per milliliter following the same protocol used for transfection experiments. The *z* average and PDI were calculated by using the automatic mode. Every sample was measured using three spectroscopic runs consisting of 10 consecutive scans (each of 10 s duration).

Stastical Analysis: All measurements for in vitro experiments were collected ($n=3$–5) and expressed as means ± standard deviation. One-way ANOVA was used in conclusion with Bonferoni's multiple comparison test to assess the statistical significance.

Acknowledgements

This work was supported by the Max Planck Society and the Alexander von Humboldt Foundation (M.N.A.). We thank HASYLAB, Hamburg, Germany, for beam time and for providing excellent facilities and support.

Keywords: DNA · lipids · monolayers · transfection · X-ray scattering

[1] M. E. A. Downs, S. Kobayashi, I. Karube, *Anal. Lett.* **1987**, *20*, 1897–1987.
[2] Z. Junhui, C. Hong, Y. Ruifl, *Biotechnol. Adv.* **1997**, *15*, 43–58.
[3] J. Wang, *Nucleic Acids Res.* **2000**, *28*, 3011–3016.
[4] F. C. Simmel, W. U. Dittmer, *Small* **2005**, *1*, 284–299.
[5] M. Artemyev, D. Kisiel, S. Abmiotko, M. N. Antipina, G. B. Khomutov, V. V. Kislov, A. A. Rakhnyanskaya, *J. Am. Chem. Soc.* **2004**, *126*, 10594–10597.
[6] W. F. Anderson, *Nature* **1998**, *392*, 25–30.
[7] R. A. Stull, F. C. Szoka, *Pharm. Res.* **1995**, *12*, 465–483.
[8] S. D. Patil, D. J. Burgess, *AAPS Newsmagazine* **2003**, 6.
[9] K. K. Hunt, S. A. Vorburger, *Science* **2002**, *297*, 415–416.
[10] J. Sen, A. Chaudhuri, *J. Med. Chem.* **2005**, *48*, 812–820.
[11] A. Aissaoui, B. Martin, E. Kan, N. Oudrhiri, M. Hauchecorne, J. P. Vigneron, J. M. Lehn, *J. Med. Chem.* **2004**, *47*, 5210–5223.
[12] G. B. Sukhorukov, L. A. Feigin, M. M. Montrel, B. I. Sukhorukov, *Thin Solid Films* **1995**, *259*, 79–84.
[13] G. B. Sukhorukov, M. M. Monterl, A. I. Petrov, L. I. Shabarchina, B. I. Sukhorukov, *Biosens. Bioelectron.* **1996**, *11*, 913–922.
[14] Y. Okahata, K. Tanaka, *Thin Solid Films* **1996**, *284–285*, 6–8.
[15] M. M. Montrel, G. B. Sukhorukov, A. I. Petrov, L. I. Shabarchina, B. I. Sukhorukov, *Sens. Actuators, B* **1997**, *42*, 225–231.
[16] K. Kago, H. Matsuoka, R. Yoshitome, H. Yamaoka, K. Ijiro, M. Shimomura, *Langmuir* **1999**, *15*, 5193–5196.
[17] M. Sastry, V. Ramakrishnan, M. Pattarkine, K. N. Ganesh, *J. Phys. Chem. B* **2001**, *105*, 4409–4414.
[18] V. Ramakrishnan, M. D'Costa, K. N. Ganesh, M. Sastry, *Langmuir* **2002**, *18*, 6307–6311.
[19] V. Ramakrishnan, M. D'Costa, K. N. Ganesh, M. Sastry, *J. Colloid Interface Sci.* **2004**, *276*, 77–84.
[20] S. Erokhina, T. Berzina, L. Cristofolini, O. Konovalov, V. Erokhin, M. P. Fontana, *Langmuir* **2007**, *23*, 4414–4420.
[21] S. Gromelski, G. Brezesinski, *Langmuir* **2006**, *22*, 6293–6301.
[22] S. D. Patil, D. G. Rhodes, D. J. Burgess, *AAPS J.* **2005**, *7*, E61-E77.
[23] M. N. Antipina, B. Dobner, O. V. Konovalov, V. L. Shapovalov, G. Brezesinski, *J. Phys. Chem. B* **2007**, *111*, 13845–13850.
[24] M. Antipina, I. Schulze, B. Dobner, A. Langner, G. Brezesinski, *Langmuir* **2007**, *23* 3919–3936.
[25] J. H. Felgner, R. Kumar, C. N. Sridhar, C. J. Wheeler, Y. J. Tsai, R. Border, P. Ramsey, M. Martin, P. L. Felgner, *J Biol Chem.* **1994**, *269*, 2550–2561.
[26] H. E. J. Hofland, L. Shephard, S. M. Sullivan, *Proc. Natl. Acad. Sci. USA* **1996**, *93*, 7305–7309.
[27] J. P. Slotte, *Biochim. Biophys. Acta, Biomembr.* **1995**, 1238, 118–126.
[28] J. P. Slotte, *Biochim. Biophys. Acta, Biomembr.* **1995**, 1237, 127–134.
[29] J. P. Hagen, H. M. McConnell *Biochim. Biophys. Acta Biomembr.* **1997**, *1329*, 7–11.
[30] S. Neidle, *Oxford Handbook of Nucleic Acid Structure*, Oxford University Press, Oxford **1999**.
[31] A. D. Bates, A. Maxwell, *DNA Topology*, Oxford University Press, Oxford **2005**, p. 109.
[32] R. R. Schmidt, K. Jankowski, *Liebigs Ann.* **1996**, 867–879.
[33] F. L. Breusch, E. Ulusey, *Chem. Ber.* **1953**, *86*, 688–692.
[34] J. Als-Nielsen, D. Jacquemain, K. Kjaer, M. Lahav, F. Levellier, L. Leiserowitz, *Phys. Rep.* **1994**, *246*, 251–313.
[35] D. Jacquemain, F. Leveiller, S. Weinbach, M. Lahav, L. Leiserowitz, K. Kjaer, J. Als-Nielsen, *J. Am. Chem. Soc.* **1991**, *113*, 7684–7691.
[36] V. M. Kaganer, H. Möhwald, P. Dutta, *Rev. Mod. Phys.* **1999**, *71*, 779–819.
[37] K. Kjaer, *Physica B* **1994**, *198*,100–109.
[38] R. Rietz, W. Rettig, G. Brezesinski, W. G. Bouwman, K. Kjaer, H. Möhwald, *Thin Solid Films* **1996**, *285*, 211–215.
[39] C. Symietz, M. Schneider, G. Brezesinski, H. Möhwald, *Macromolecules* **2004**, *37*, 3865–3875.
[40] T. R. Jensen, K. Kjaer, *Structural Properties and Interactions of Thin Films at the Air-Liquid Interface Explored by Synchrotron Scattering in Novel Methods to Study Interfacial Layers* (Ed. R. Miller) Elsevier, Amsterdam **2001**, 205–254.
[41] I. Weissbuch, R. Popovitz-Biro, M. Lahav, L. Leiserowitz, K. Kjaer, J. Als-Nielsen, *Adv. Chem. Phys.* **1997**, *102*, 39–120.
[42] J. S. Pedersen, *J. Appl. Crystallogr.* **1992**, *25*, 129–145.
[43] I. W. Hamley, J. S. Pedersen, *J. Appl. Crystallogr.* **1994**, *27*, 29–35.
[44] J. S. Pedersen, I. W. Hamley, *J. Appl. Crystallogr.* **1994**, *27*, 36–49.
[45] M. Schalke, M. Lösche, *Adv. Colloid Interface Sci.* **2000**, *88*, 243–274.
[46] M. Schalke, P. Krüger, M. Weygand, M. Lösche, *Biochim. Biophys. Acta Biomembr.* **2000**, *1464*, 113–126.
[47] C. A. Helm, H. Möhwald, K. Kjaer, J. Als-Nielsen, Europhys. Lett. **1987**, *4*, 697–703.
[48] A. D. Miller, *Angew. Chem.* **1998**, *110*, 1862–1880; *Angew. Chem. Int. Ed.* **1998**, *37*, 1768–1785.
[49] J. Sen, A. Chaudhuri, *J. Med. Chem.* **2005**, *48*, 812–820.
[50] D. D. Lasic, *Liposomes in Gene Delivery* CRC Press, Boca Raton, FL, **1997**.
[51] R. N. Hull, W. R. Cherry, *In Vitro* **1976**, *12*, 670–677.
[52] Quiagen® Plasmid Purification handbook, www1.qiagen.com/Plasmid/handbooks.aspx.
[53] V. M. Yenugonda, R. Mukthavaram, A. Chaudhuri, *J. Med. Chem.* **2004**, 47, 3938–3948.
[54] I. M. Rosenberg, *Protein Analysis and Purification: Benchtop Techniques*, Bikhäuser, Boston **1996**.
[55] T. Mosmann, *J. Immunol. Methods* **1983**, *65*, 55–63.

Received: January 30, 2009
Published online on September 3, 2009

